JOURNAL OF CATALYSIS **178,** 395–407 (1998)
ARTICLE NO. CA982169

Elucidation of Lean-NO_x Reduction Mechanism Using Kinetic Isotope Effect

Byong K. Cho[1]

Physics and Physical Chemistry Department, General Motors Research & Development Center, Warren, Michigan 48090-9055

Received April 28, 1997; revised January 14, 1998; accepted May 29, 1998

The effect of an NO isotope on the kinetics of lean-NOx catalysis in ($NO + C_2H_4 + O_2$) reaction mixtures over Pt-ZSM-5 was theoretically analyzed and compared with experimental data obtained with a fixed-bed plug-flow reactor. The large kinetic isotope effect, as well as kinetic oscillations observed previously, was explained by NO decomposition kinetics on Pt surfaces which undergo phase transition between (1×1) and (hex) phases induced by adsorbed reactant species. Results indicate the importance of NO decomposition kinetics in lean-NO_x catalysis, lending further support to a lean-NO_x reduction mechanism which involves NO decomposition accompanied by hydrocarbon oxidation.

INTRODUCTION

Catalytic reduction of NO by hydrocarbons under highly oxidizing conditions has been investigated extensively in recent years (e.g., (1–27)). Substrates of lean-NO_x catalysts reported so far in the literature are based mostly on zeolite materials with a few exceptions (e.g., (20, 22, 24, 26)). For active ingredients, both base metal catalysts (such as Cu, Co, and Fe) and noble metal catalysts (such as Pt, Rh, and Ir) have been investigated. Catalytic activity measurements have indicated that base metal catalysts are suitable for high temperature applications such as lean-burn gasoline engines, whereas noble metal catalysts are for low temperature applications such as diesel engines, due to differences in their lightoff temperatures for lean-NO_x reduction (26).

Despite numerous reports on reactivity measurements in the literature, the reaction mechanism of lean-NO_x catalysis remains controversial. Apparently, the controversy is due largely to the fact that the rate-determining step of the lean-NO_x catalysis is either unknown or changing, depending upon the type of catalysts and reaction conditions. For example, the rate-determining steps proposed in the literature for Cu-ZSM-5 include the following:

—NO decomposition (10, 22)
—NO_2 formation via $NO + O_2$ reaction (13, 19)
—Formation of partially oxidized hydrocarbons (13)
—Formation of organic nitrosyl compounds (12)
—Formation of carbonaceous deposits (8, 13).

Currently, the most widespread production lean-burn engine is the diesel engine. Pt-based lean-NO_x catalysts are promising, especially for diesel engines, in view of their superior durability and lightoff characteristics to their Cu-based counterparts. For this reason, we have been focusing on investigation of Pt-ZSM-5 and Pt/Al_2O_3 for lean-NO_x reduction. The most plausible reaction mechanism for the lean-NO_x reduction over Pt-ZSM-5 has been proposed to be the combination of NO decomposition and the hydrocarbon oxidation (1, 21, 22, 26, 27).

In a more recent study of the lean-NO_x catalysis over Pt-ZSM-5, sustained kinetic oscillations were observed under steady-state operating conditions, along with the unusually large effect of an NO isotope on lean-NO_x reduction kinetics (1). Although the kinetic oscillations were qualitatively explained by both the surface phase-transition model and the surface regeneration model, the kinetic isotope effect could not be explained by the conventional zero-point vibrational energy argument (1). (It is noteworthy that similar kinetic oscillations were also observed for $NO + O_2 + C_3H_6$ reaction over alumina (28) at high temperatures around 490–530°C.) This unexplained strong kinetic effect of an NO isotope on lean-NO_x catalysis observed over Pt-ZSM-5 is not only of fundamental interest but of practical importance in understanding the kinetic mechanism of lean-NO_x catalysis over noble metal surfaces in general, as will be shown in this paper.

In this work, we analyze the lean-NO_x reduction performance of a microreactor containing Pt-ZSM-5 using a simplified kinetic model combined with a reactor model. Results of kinetic analysis are compared with experimental data obtained for the ($NO + C_2H_4 + O_2$) reaction system with and without using isotopically labeled NO. Our purpose is to provide an explanation for the unusually strong kinetic isotope effect, which may in turn help us ascertain a correct reaction mechanism for the lean-NO_x catalysis.

[1] E-mail: bcho@notes.gmr.com.

0021-9517/98 $25.00

FORMULATION OF A MODEL FOR LEAN-NO_x REDUCTION

Kinetic Model Based on Dichotomy of Surface Sites

For NO reduction with hydrocarbons under lean conditions over noble-metal-based catalysts, it has been proposed that the lean-NO_x catalysis proceeds with NO decomposition, in combination with HC oxidation (1, 21, 22, 26). Also, a strong inhibition effect of NO on lean-NO_x catalysis over Pt-ZSM-5 indicates that NO decomposition is the rate-determining step around the reaction lightoff temperature, where the kinetic isotope effects are observed (1, 26). In view of these observations, we focus on the NO decomposition part of the lean-NO_x catalysis in the ($NO + C_2H_4 + O_2$) reaction system, since our interest in this work is in the NO isotope effect. Assuming all the Pt surface sites are equally accessible to NO, C_2H_4, and O_2, we describe the NO decomposition rate using two different kinetic models: the conventional Langmuir–Hinshelwood (LH) model and the surface vacancy (SV) model.

For steady-state kinetic analysis, it is convenient to divide the total surface sites into two sets of mutually exclusive surface sites at a given moment; they are collectively designated as sites A and B as shown in Fig. 1, where the A-sites are defined as a collection of surface sites on which NO adsorption/desorption and decomposition occur at the given moment, while the B-sites are a collection of the rest of the surface sites occupied by N, O, or C_2H_4. The characteristics of these two sites can be described as follows:

- NO decomposition occurs on A-sites which include both NO adsorption sites and vacant sites necessary for NO decomposition. By the definition of the B-sites, the products of NO decomposition—namely, O and N atoms—are supposed to occupy the B-sites and are either scavenged by C_2H_4 or desorb as N_2 (or N_2O).
- Oxygen from both NO and the gas-phase O_2 is the source for the adsorbed oxygen on the B-sites.
- C_2H_4 oxidation occurs on B-sites, generating vacant sites which may remain as B-sites by adsorbing C_2H_4 (or O_2), or may convert to A-sites by adsorbing NO.

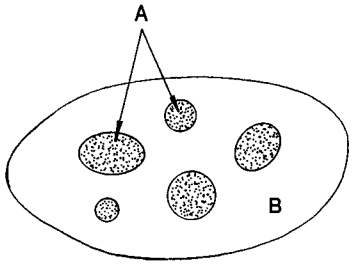

FIG. 1. Conceptual dichotomy of catalytic surfaces. (A-sites = surface sites occupied by NO or vacant; B-sites = surface sites occupied by C_2H_4, O, or N.)

Note that, in this reaction mechanism, interchange is possible between the A-sites and the B-sites during the course of lean-NO_x reduction. For example, the A-sites may convert to the B-sites on decomposing NO, whereas the B-sites may convert back to the A-sites depending on the rate of NO adsorption relative to the rate of C_2H_4 adsorption. Although the sum of the surface area of A-sites (σ_A) and that of B-sites (σ_B) remains constant (equal to the total surface area σ), the surface area ratio (σ_A/σ_B) may vary with the changing experimental conditions.

The kinetic effect of NO isotope substitution on the B-sites (where NO decomposition products adsorb) is negligible due to the fact that the NO concentration is very low, compared with the O_2 and C_2H_4 concentrations in the ($NO + C_2H_4 + O_2$) reaction system considered in this work (1), in combination with the fact that the difference in the intrinsic decomposition rate between ^{14}NO and ^{15}NO is very small (1). In other words, the kinetic effect of the NO isotope substitution in this ($NO + C_2H_4 + O_2$) reaction system is essentially confined in the A-sites. Thus, the idea behind the concept of dichotomized surface sites adopted here is to separate the NO decomposition process on the A-sites (which is directly affected by the NO isotope substitution) from the C_2H_4 oxidation process on the B-sites (which is virtually unaffected by the NO isotope substitution) during lean-NO_x catalysis.

LH model. Following the conventional Langmuir–Hinshelwood kinetic mechanism, the NO decomposition rate (R) on catalytic surfaces under steady-state conditions can in general be written as

$$R = k'\theta_{NO}\theta_V, \qquad [1]$$

where

$$\theta_V = 1 - \theta_O - \theta_{HC} - \theta_{NO} - \theta_N, \qquad [2]$$

and θ_O, θ_{HC}, θ_{NO}, θ_N, and θ_V are the surface coverages of oxygen, HC, NO, N, and vacancy, respectively, based on the total surface area of the catalyst. For further kinetic analysis of NO decomposition during lean-NO_x catalysis, we introduce the concept of normalized surface coverages, which is based on the surface area of type A sites (as opposed to the conventional concept of surface coverages based on the total surface area). In this definition, the normalized surface coverage of NO (ϕ_{NO}) and vacancy (ϕ_V) can be expressed as

$$\phi_{NO} = \theta_{NO}/(1 - \theta_O - \theta_{HC} - \theta_N), \qquad [3]$$

$$\phi_V = \theta_V/(1 - \theta_O - \theta_{HC} - \theta_N). \qquad [4]$$

Assuming adsorption/desorption equilibrium for NO on the surface of the type A sites, it can be shown (Appendix B)

that

$$\phi_{NO} = KC/(1 + KC) \quad [5]$$

$$\phi_V = 1/(1 + KC) \quad [6]$$

and the NO decomposition rate on the surface can be rewritten in terms of the normalized surface coverages as

$$R = k\phi_{NO}\phi_V, \quad [7]$$

where k is the rate constant for NO decomposition based on the normalized surface coverages. That is, Eq. [7] describes the NO decomposition kinetics on the A-sites in Fig. 1 using the conventional LH mechanism.

Surface vacancy model. Under steady-state conditions of lean-NO_x catalysis around the reaction lightoff temperature, it is reasonable to assume that the catalyst surface of type A sites is covered predominantly by NO with very few vacant surface sites available. In this case, $\phi_{NO} \approx 1$ and thus the rate of NO decomposition (R) becomes directly proportional to the availability of the surface vacancy. That is,

$$R = k\phi_V, \quad [8]$$

which we call the *surface vacancy (SV) model.* Note that the SV model is a special case of the LH model with $\phi_{NO} \to 1$.

Reactor Model

A packed-bed microreactor containing small catalyst powder under isothermal steady-state operating conditions can be described by a plug-flow reactor model;

$$Q(dC/d\xi) = -\sigma_A R \quad [9]$$

with the feed condition

$$C = C_i \quad \text{at } \xi = 0, \quad [10]$$

where C is the gas-phase NO concentration, Q is the volumetric feed flow rate, R is the rate expression for NO decomposition, and ξ is the dimensionless axial distance along the reactor length.

KINETIC ANALYSIS OF ISOTOPE EFFECT

The primary isotope effect on the kinetics of lean-NO_x catalysis manifests itself in the intrinsic rate of NO decomposition due to the zero-point energy difference between isotopic molecules, with the secondary effect induced by changes in surface coverages of reactant species originating from the primary isotope effect. Thus, the primary and secondary effects are inherently related to produce the overall kinetic isotope effect. (Although the adsorptive isotope effect (i.e., the isotope effect on adsorption equilibrium constant) is assumed negligible for the moment, it will be discussed later in qualitative terms.)

Primary Effect on the Rate Constant of NO Decomposition

The primary effect of an isotopic NO on the rate constant for NO decomposition can be expressed in terms of the zero-point vibrational wave number by (29)

$$\frac{k^*}{k} = \sinh\left(\frac{hc\nu^*}{2\kappa T}\right) \Big/ \sinh\left(\frac{hc\nu}{2\kappa T}\right), \quad [11]$$

where k and k^* denote the decomposition rate constants of ^{14}NO and ^{15}NO, respectively. The vibrational wave number of ^{15}NO adsorbed on Pt surfaces (ν^*) can be calculated from the vibrational frequency of ^{14}NO (ν) by

$$\frac{\nu^*}{\nu} = \sqrt{\frac{\mu}{\mu^*}}, \quad [12]$$

where μ and μ^* are the reduced masses of ^{14}NO and ^{15}NO, respectively. It should be noted that this primary effect is universally applicable regardless of the kinetic model employed.

Overall Isotope Effect on Lean-NO_x Reduction Kinetics

The overall isotope effect, which results from a combination of the primary and secondary effects, can be analyzed most efficiently by employing two models discussed earlier for NO decomposition: the LH model and SV model.

LH model for NO decomposition. Combining the reactor model (Eqs. [9]) with the kinetic model (Eqs. [5], [6], and [7]) gives

$$Q\frac{dC}{d\xi} = -\frac{\sigma_A kKC}{(1 + KC)^2} \quad [13]$$

which can be integrated using the feed condition (Eq. [10]) and the reactor-average value of σ_A (i.e., $\langle\sigma_A\rangle$) to yield

$$\frac{1}{2}[(2 + KC_i)^2 - \{2 + KC(\xi)\}^2] + \ln\left(\frac{C_i}{C(\xi)}\right) = \alpha\xi, \quad [14]$$

where α is the dimensionless rate constant for NO decomposition defined by

$$\alpha = \langle\sigma_A\rangle kK/Q. \quad [15]$$

Use of $\langle\sigma_A\rangle$ for the integration of Eq. [13] is a reasonable approximation, considering that the surface area of A-sites is only weakly dependent on the gas-phase reactant concentrations due to the overwhelming excess amount of oxygen whose concentration is virtually constant along the reactor length. This approximation is thus believed to be quite adequate for the purpose of investigating the NO isotope effect.

In particular, at the reactor outlet, Eq. [14] reduces to

$$\frac{1}{2}[(2 + KC_i)^2 - \{2 + KC_i(1 - x)\}^2] - \ln(1 - x) = \alpha. \quad [16]$$

Equation [16] represents the relation between α and the NO conversion at the reactor outlet for the NO decomposition reaction following the LH kinetic model in a plug-flow reactor. When ordinary NO (^{14}NO) is replaced by isotopic *NO (^{15}NO, for example), the decomposition rate constant undergoes a small change according to Eq. [11], which in turn brings a change in α due to Eq. [15], leading eventually to a change in the NO conversion according to Eq. [16]. (For convenience hereinafter, the superscript $*$ denotes the isotopic ^{15}NO.) The kinetic effect of this small change in the decomposition rate constant due to the NO isotope can be analyzed using a perturbation technique, noting that

$$\alpha^* = \alpha + \delta\alpha, \qquad [17]$$

$$x^* = x + \delta x, \qquad [18]$$

where $\delta\alpha$ and δx are small perturbation in the dimensionless rate constant (α) and the NO conversion (x), respectively, resulting from the ^{15}NO isotope. Inserting Eqs. [17] and [18] into Eq. [16], it can be shown (Appendix C) that

$$\frac{C_i^*(1-x^*)}{C_i(1-x)} = 1 + \frac{\alpha}{[1+KC_i(1-x)]^2}\left(1-\frac{k^*}{k}\right). \qquad [19]$$

When the feed NO concentration was kept constant for both regular and isotopic NO (i.e., $C_i = C_i^*$), Eq. [19] reduces to

$$\frac{1-x^*}{1-x} = 1 + \frac{\alpha}{[1+KC_i(1-x)]^2}\left(1-\frac{k^*}{k}\right) \qquad [20]$$

which shows the relation between the conversion of regular NO and that of isotope NO as a function of the primary isotope effect under otherwise identical experimental conditions. Note that Eq. [20] is applicable only when both $\delta\alpha$ and δx are much smaller than α and x, respectively, due to the nature of the first-order perturbation employed.

Surface vacancy model for NO decomposition. The reactor model (Eq. [9]), combined with the kinetic model (Eqs. [6] and [8]) yields

$$Q\frac{dC}{d\xi} = -\frac{\sigma_A k}{1+KC} \qquad [21]$$

which can be integrated in the same way as was done before for Eq. [13] to obtain

$$\frac{1}{2}[(1+KC_i)^2 - \{1+KC(\xi)\}^2] = \alpha\xi. \qquad [22]$$

Solving Eq. [22] for $KC(\xi)$, we obtain

$$KC(\xi) = -1 + \sqrt{(1+KC_i)^2 - 2\alpha\xi}. \qquad [23]$$

Similarly, when *NO was used in place of regular NO, we get from Eq. [22]

$$KC^*(\xi) = -1 + \sqrt{(1+KC_i^*)^2 - 2\alpha^*\xi}. \qquad [24]$$

Dividing Eq. [24] by Eq. [23] and assuming that the feed concentrations of NO and *NO are kept constant, it can be shown at the reactor outlet that

$$\frac{1-x^*}{1-x} = \frac{-1+\sqrt{f(\alpha^*)}}{-1+\sqrt{f(\alpha)}}, \qquad [25]$$

where

$$f(\alpha) = (1+KC_i)^2 - 2\alpha. \qquad [26]$$

If KC_i is much greater than unity, Eq. [25] reduces to

$$\frac{1-x^*}{1-x} = \sqrt{\frac{g(\alpha^*)}{g(\alpha)}}, \qquad [27]$$

with

$$g(\alpha) = (KC_i)^2 - 2\alpha. \qquad [28]$$

Equation [25] or [27] quantifies the primary isotope effect on NO conversion in lean-NO_x catalysis when the rate of NO decomposition is controlled by the availability of surface vacancy.

COMPARISON WITH EXPERIMENT

Experiments

The microreactor was made of a 0.32-cm OD stainless steel tube packed with Pt-ZSM-5 powder which was prepared from ion exchange of Pt on ZSM-5 using $Pt(NH_3)_4Cl_2$ salt as the Pt ion precursor. The Pt loading of the catalyst was 5.9 wt%, and the total amount of sample in the reactor was 1.6 mg. Steady-state activity of the reactor for NO reduction in ($NO + C_2H_4 + O_2$) mixtures was measured under isothermal steady-state conditions over the temperature range of 180–213°C, using both regular ^{14}NO and isotopic ^{15}NO. The feedstream contained 230 ppm NO, 1200 ppm C_2H_4, and 7% O_2 with balance He. All experimental conditions were kept constant, including the gas space velocity (859,000 h^{-1}), except the change between ^{14}NO and ^{15}NO in the feed gas mixture. Conversions of both ^{14}NO and ^{15}NO were monitored by a mass spectrometer calibrated using argon as the reference gas. A detailed description on the catalyst, reactor, and experimental conditions can be found elsewhere (26).

Estimation of Model Parameters

Important system parameters affecting the kinetic isotope effect can be identified from Eqs. [11], [19], and [24]. They are the thermodynamic parameters K and ν, the dimensionless kinetic parameter α, and the reactor operating parameters C_i, Q, and T. The dimensionless rate constant for decomposition of regular NO, α, can be determined from Eqs. [16] and [24], using the experimental NO conversion data at the reactor outlet. Once α is known, α^* can be estimated from Eq. [11]. The NO adsorption equilibrium

constant, K, was calculated from the k_a/k_d ratio, where k_a was estimated from the kinetic theory of adsorption for a perfect gas using a sticking coefficient of 0.6 (30), while k_d was obtained from literature data (31). In view of the possible phase transition of the Pt surface between (1×1) and (hex) phases, different values of the adsorption equilibrium constants (i.e., K_{11} and K_H for the (1×1) and (hex) phases, respectively) and decomposition rate constants [α_{11} and α_H] were assigned to each of these phases. The value of K on the (hex) phase, K_H, was approximated by that on Pt(111), since the (hex) phase is believed to have a distorted hexagonal overlayer that is similar to the Pt(111) surface (31), while the value of K_{11} was obtained from the literature data (30, 31). An exact value of the NO decomposition rate constant on the (hex) phase is not available at this time, although literature data (32) suggest that the observed NO decomposition rate on the (hex) phase is approximately one-third that on the (1×1) phase (i.e., $R_{11}/R_H \approx 3$) at 500 K. Thus, the value of α_{11} was determined from the experimental data of R_{11} obtained previously (1), while α_H was obtained from the estimated value of R_H which was assumed to be one-third that of R_{11}. The zero-point vibrational frequency of NO was taken to be 1780 cm^{-1}, based on measurements at 325 K (33). Parameter values and their sources are listed in Table 1.

Model Predictions and Comparison with Experiments

It is well documented that Pt(100) is the most stable plane on polycrystalline and supported Pt particles (34, 35) and that it undergoes phase transition from the (hex) to the (1×1) phase, induced by the adsorption of NO (30, 36, 37). The (1×1) phase is known to be much more active than the (hex) phase for NO decomposition (31, 38). Recently, it has been reported that the $NO + C_2H_4 + O_2$ system exhibits a higher activity without yielding kinetic oscillations, compared with the $^*NO + C_2H_4 + O_2$ system which yielded kinetic oscillations between higher and lower rates under exactly the same experimental conditions (1). To explain this qualitatively, it has been suggested that Pt surfaces in the Pt-ZSM-5 catalyst consist primarily of the (1×1) phase for the $NO + C_2H_4 + O_2$ system, while it may fluctuate between the (1×1) and the (hex) phases for the $^*NO + C_2H_4 + O_2$ system (1). In the sections below, the validity of this hypothesis is examined quantitatively through model simulations and comparison with experiments.

TABLE 1

Model Parameters for Kinetic Analysis of Isotope Effects

Parameter	Used in this work	References
C_i	5.9239×10^{-9} mol/cm^3 at 200°C	This work
k^*/k	Eq. [11]	(29)
K_{11}	$1.8546 \times 10^{-5} \sqrt{T} \exp(36{,}000/{}^*R_gT)$	(31)
α_{11}	Estimated from NO conversion data	(1)
α^*_{11}	$\alpha_{11}k^*/k$	This work
K_H	$1.8546 \times 10^{-5} \sqrt{T} \exp(25{,}000/{}^*R_gT)$	(31)
α_H	Estimated from α_{11} and Ref. (32)	(32)
α^*_H	$\alpha_H k^*/k$	This work
Q	0.8333 cm^3/s at 25°C	This work
ν	1780 cm^{-1}	(33)

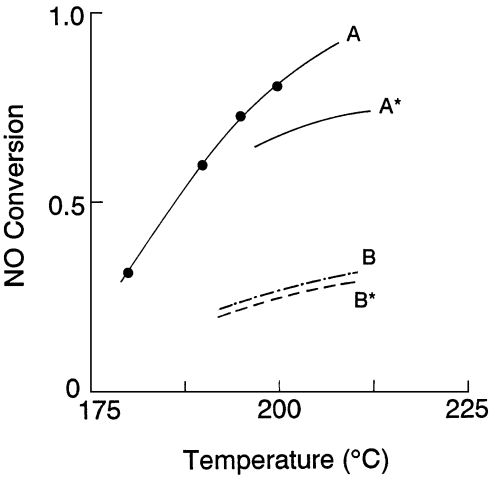

FIG. 2. Model predictions of kinetic isotope effect: A = experimental data with $(NO + C_2H_4 + O_2)$ reaction assumed to be occurring on (1×1) phase; A* = model prediction with $(^*NO + C_2H_4 + O_2)$ reaction on (1×1) phase; B = estimated NO conversion for $(NO + C_2H_4 + O_2)$ reaction on (hex) phase; B* = model prediction with $(^*NO + C_2H_4 + O_2)$ reaction on (hex) phase.

Kinetic isotope effect on the (1×1) phase. Due to strong adsorption of NO on the (1×1) phase, the value of the dimensionless quantity $K_{11}C$ is much greater than unity, resulting in ϕ_{NO} close to unity. Under this condition, the NO decomposition kinetics can be described adequately by the surface vacancy model (Eq. [8]) which is a simplified version of the LH model (Eq. [7]). Model predictions obtained from Eq. [25] are shown in Fig. 2, where the conversions of NO and $^*NO$ under the same experimental conditions are compared as a function of temperature. The experimental data in Fig. 2 (curve A) were found to be consistent with the model prediction based on the NO decomposition rate on (1×1) phase estimated from the literature (32), and thus were assigned to the (1×1) phase. The $^*NO$ conversion above 200°C (curve A*) was calculated based on the estimated value of α, obtained by extrapolating the NO conversion data (curve A) beyond 200°C. Clearly, the activity of the catalyst decreases much more than the decrease in k predicted (1) by the zero-point vibrational energy through Eq. [11].

Kinetic isotope effect on the (hex) phase. The adsorption of NO on the (hex) phase is much weaker than that on the (1×1) phase. The magnitude of K_HC for the (hex) phase is comparable to unity, and the NO decomposition kinetics can be described by the LH model, Eq. [7]. In the absence of

experimental data for the ($NO + C_2H_4 + O_2$) system over the (hex) phase, the NO conversion over the (hex) phase was estimated to be a third that over the (1×1) phase (i.e., $R_{11}/R_H \approx 3$) as shown in curve B in Fig. 2, assuming the overall rate is controlled by the rate of NO decomposition (32). Shown also in Fig. 2 are the model predictions for the *NO conversion over the (hex) phase (curve B*), in comparison with the measured NO and calculated *NO conversion over the (1×1) phase (curve A and A*). As expected, the *NO conversion over the (hex) phase (curve B*) is much lower than the NO conversion over the (1×1) phase (curve A). Obviously, this large difference can be attributed to the combination of two factors: the NO isotope effect and the surface phase transition. It is noted, however, that the (1×1) phase exhibits much stronger isotope effect than the (hex) phase.

Comparison: model vs experiments. Figure 3 compares the model predictions of the activity of both the (1×1) and the (hex) phases for the ($*NO + C_2H_4 + O_2$) reaction system with experimental data showing kinetic oscillations. Clearly, the NO conversion data on the upper branch agree reasonably well with those predicted by the (1×1) phase model, while the lower branch data can be described by the (hex) phase model. Thus, the kinetic oscillation observed for the ($*NO + C_2H_4 + O_2$) system over Pt-ZSM-5 can be explained quantitatively by the phase transition between the (1×1) and the (hex) phase as suggested previously (1).

Determination of Dimensionless Rate Constant for NO Decomposition

Presented in Fig. 4 are the dimensionless rate constants for NO decomposition over the (1×1) and (hex) phases, α_{11} and α_H respectively, determined from Eq. [16] using the experimental data on NO conversion. It is noted that α_{11} is greater than α_H by nearly 10 orders of magnitude. The

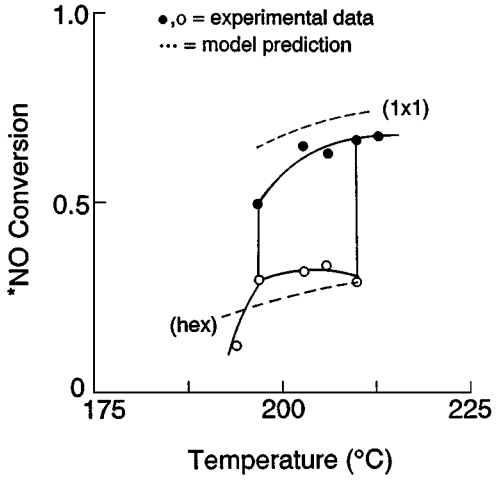

FIG. 3. Comparison of model predictions with experimental data for the ($*NO + C_2H_4 + O_2$) reaction system.

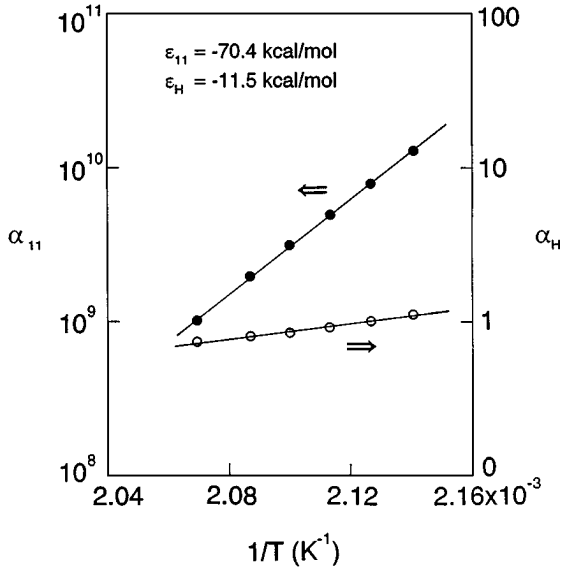

FIG. 4. Dimensionless rate constant for NO decomposition.

activation energies for α_{11} and α_H obtained from the slopes of the straight lines in Fig. 4 are

$$\varepsilon_{11} = -70.4 \text{ kcal/mol} \quad \text{for } \alpha_{11},$$

$$\varepsilon_H = -11.5 \text{ kcal/mol} \quad \text{for } \alpha_H.$$

The negative activation energy is indicative of a decreasing rate of overall NO decomposition with increasing temperature. This can be explained by the fact that the dimensionless rate constant contains two other temperature-dependent parameters in addition to k; namely, K and $\langle\sigma_A\rangle$ (see Eq. [15]). The adsorption equilibrium constant, K, decreases with temperature, and so does $\langle\sigma_A\rangle$, due to the rate of C_2H_4 oxidation increasing with temperature faster than the rate of NO decomposition. The important role of K and $\langle\sigma_A\rangle$ in determining the observed rate of NO decomposition is evident from the negative activation energy of the overall dimensionless rate constant.

Figure 5 shows the overall rate constants (both $\langle\sigma_A\rangle k_{11}$ and $\langle\sigma_A\rangle k_H$) calculated from Fig. 4 using the values of K_{11} and K_H in Table 1. The overall rate constant for NO decomposition over the (1×1) phase, which is in line with the literature values (32), is greater than that over the (hex) phase by 4–5 orders of magnitude. Interestingly, the former exhibits a negative activation energy, while the latter a positive one:

$$E_{11} = -33.9 \text{ kcal/mol},$$

$$E_H = 14.5 \text{ kcal/mol}.$$

We propose that the negative activation energy (E_{11}) may be attributed to the temperature-dependent nature of $\langle\sigma_A\rangle$, as follows: It is reasonable to assume that the surface area of type-A sites on Pt is inversely proportional to the rate

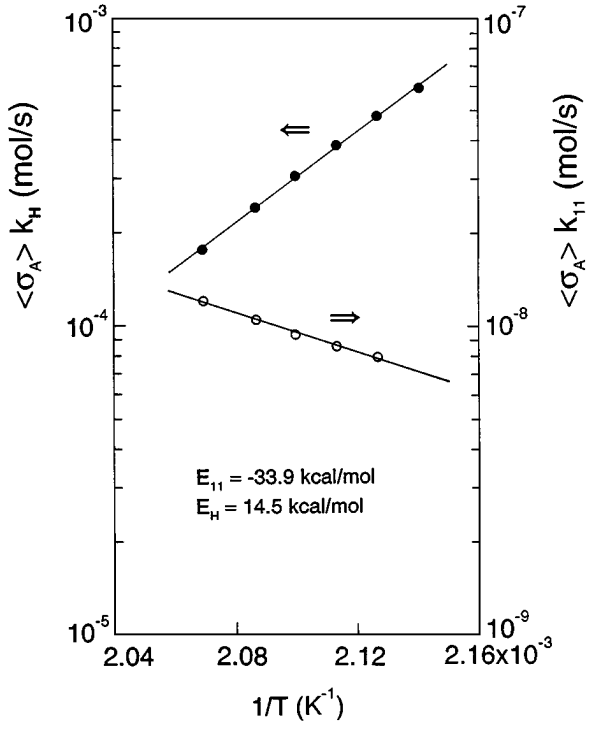

FIG. 5. Overall rate constant for NO decomposition.

of C_2H_4 oxidation by oxygen. Since the activation energy of C_2H_4 oxidation is 58.6 kcal/mol (40), the true activation energy of NO decomposition on the (1×1) phase can be estimated to be 24.7 kcal/mol (i.e., $58.6 - 33.9 = 24.7$, where 58.6 is due to $\langle\sigma_A\rangle$ assumed to be inversely proportional to the rate of C_2H_4 oxidation) which is in line with the literature value of 28.5 kcal/mol (39). The activation energy for NO decomposition over the (hex) phase, E_H is in line with other literature data where very slow rates of NO decomposition were observed over polycrystalline or supported Pt surfaces (32).

Axial Profiles of Surface Coverage and NO Conversion

Shown in Figs. 6a and 6b are the axial profiles of surface coverage of NO and vacancy, respectively, obtained from Eqs. [5], [6], and [14] at temperatures of 197 and 210°C for the (hex) phase. The NO surface coverage decreases gradually with the axial distance in the reactor at a given temperature, and it increases with a decrease in temperature (Fig. 6a). In the temperature range between 197 and 210°C, the reactor-average θ_{NO}^* is approximately 0.4 which closely matches the critical θ_{NO} at which a phase transition occurs between the (1×1) and (hex) phases (39). The surface vacancy increases with temperature and the axial distance in the reactor (Fig. 6b). Note that θ_{NO} and θ_V on the (hex) phase are comparable in magnitude.

On the (1×1) phase, the NO surface coverage is close to unity with a decreasing profile along the reactor length, leaving the surface vacancy extremely small on the order of 10^{-5} (Fig. 7) which was obtained from Eqs. [5], [6], and [23]. It is interesting to note that the surface vacancy increases exponentially along the axial distance in the reactor. Since the (1×1)-to-(hex) phase transition is known to occur at a lower NO surface coverage than the (hex)-to-(1×1) phase transition (32), the monotonically decreasing θ_{NO} along the

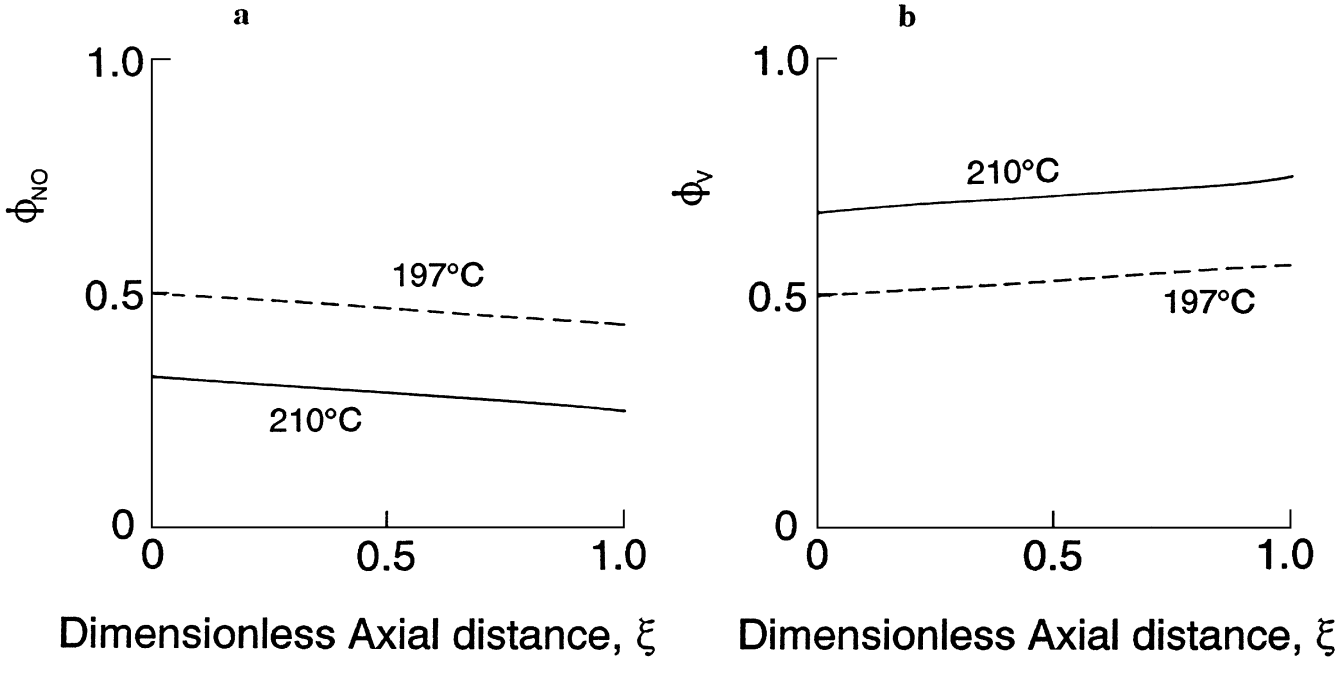

FIG. 6. Axial profile of normalized surface vacancy and NO coverage for (hex) phase.

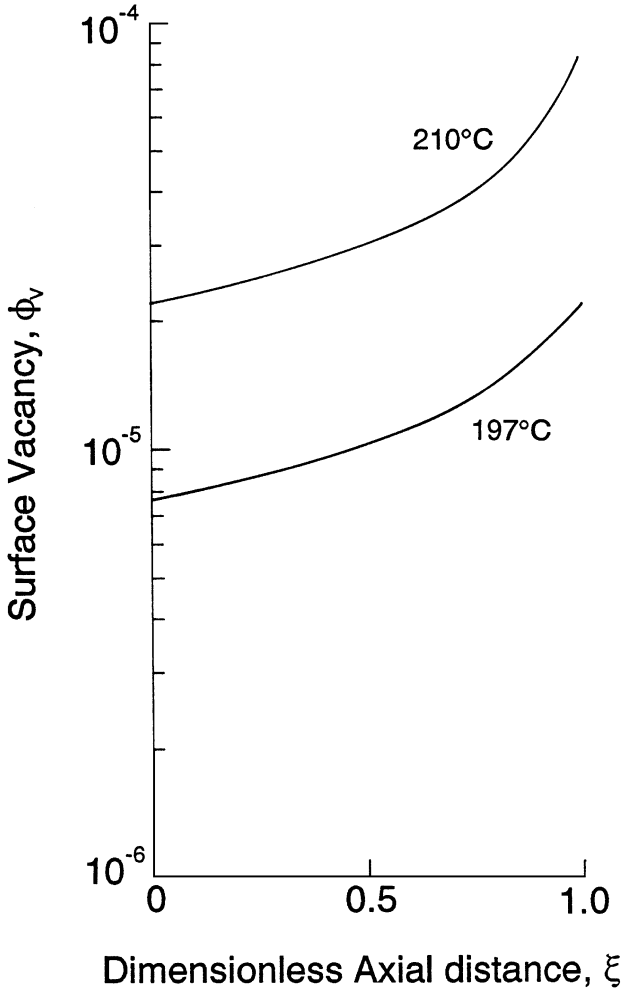

FIG. 7. Axial profile of normalized surface vacancy for (1×1) phase.

reactor length suggests that the transition from the (1×1) to (hex) phase should be favored in the downstream section of the reactor. As a result, the upstream section of the reactor can be in the (1×1) phase while the downstream section is predominantly populated by the (hex) phase. This complex distribution of surface phases may be, at least, partially responsible for the oscillation pattern observed previously (1).

Calculated using Eqs. [20] and [25] for the (hex) and (1×1) phase, respectively, Figs. 8a and 8b show the $^*NO$ conversion profiles along the axial distance in the reactor at 197 and 210°C. Note that the difference in NO conversion activity between the (1×1) and (hex) phases increases with the axial distance in the reactor, due to the cumulative effect along the reactor length of the intrinsic activity difference between the two phases.

DISCUSSION

Kinetic Model and Reaction Mechanism

By normalizing the dichotomized surface coverages, reduction of NO in the $(NO + C_2H_4 + O_2)$ system over Pt-ZSM-5 was described by the NO decomposition model allowing for transitions between the (1×1) and (hex) phases of Pt surfaces to analyze the kinetic isotope effect. Results of the model simulations are in good quantitative agreement with the experimental data; the upper limit of the kinetic oscillation can be described by the surface vacancy (SV) model on the (1×1) phase, while the lower limit by the Langmuir–Hinshelwood (LH) model on the (hex) phase. Success of the NO decomposition model in predicting the NO isotope effect in lean-NO_x catalysis supports the previously proposed reaction mechanism which involves NO decomposition followed by HC oxidation. This does not

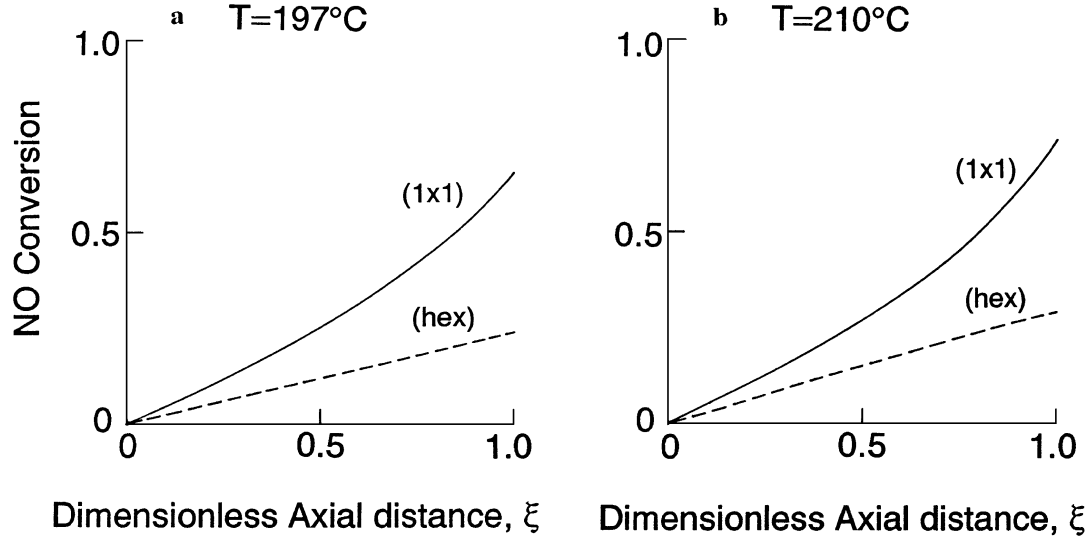

FIG. 8. Axial profile of NO conversion for the $(^*NO + C_2H_4 + O_2)$ system.

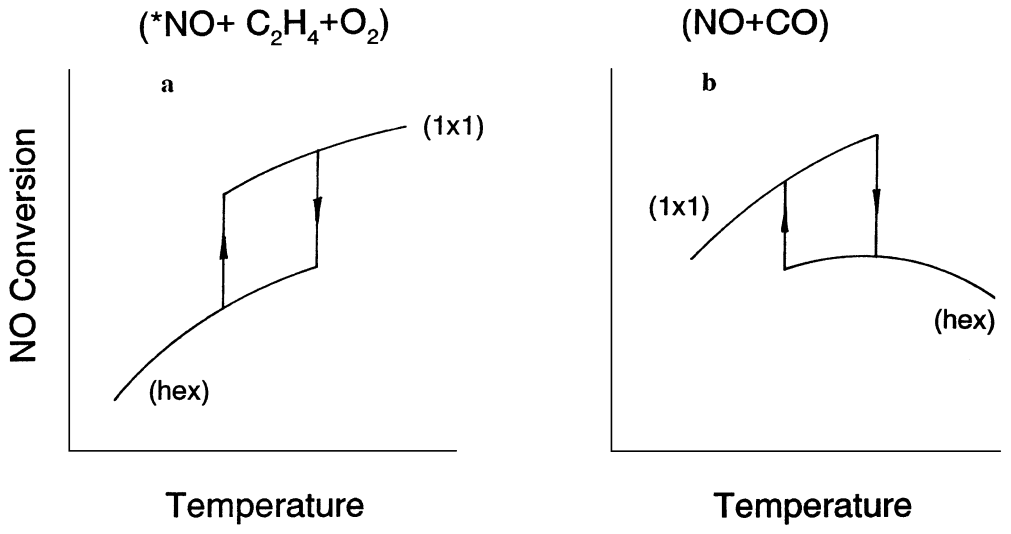

FIG. 9. Comparison of phase transition behavior between ($^*NO + C_2H_4 + O_2$) and ($NO + CO$) systems.

exclude, however, the possibility of the $2NO + O_2 \rightarrow 2NO_2$ pathway as the rate-determining step of the lean-NO_x catalysis (13, 19). It is noteworthy, however, that on Pt surfaces all NO_2 formed decomposes only to NO (41, 42). Thus, even with NO_2 formation, the rate-limiting step of the lean-NO_x catalysis could still be NO decomposition, if the thermodynamic equilibrium between NO and NO_2 (i.e., $2NO + O_2 \leftrightarrow 2NO_2$) is fast compared with the NO decomposition rate. This hypothesis is in accordance with literature reports that the NO_2 formation via ($NO + O_2$) reaction is not important in lean-NO_x catalysis over Cu-ZSM-5 and Pt/Al_2O_3 (43, 44).

For further elucidation of the reaction mechanism, the rates of ($NO + C_2H_4$) and ($NO_2 + C_2H_4$) reactions were compared over 0.9 wt% Pt-ZSM-5 catalyst. The amount of this catalyst used in the reactor experiment was determined in such a way that the total amount of Pt in the reactor remains the same as that in the previous oscillation experiments (1). Except for the absence of O_2 in the feed reactant mixture, the reactor and its operating conditions were essentially the same as those reported previously (1). Results shown in Fig. 10 indicate that the NO conversion lights off at around 400°C in both reaction systems, which is substantially higher than that (≈200°C) observed in the presence of excess O_2 (1, 26). Below the reaction lightoff temperature the rates of both reactions are essentially identical, while above the lightoff temperature the ($NO + C_2H_4$) reaction becomes faster than the ($NO_2 + C_2H_4$) reaction. This clearly demonstrates that the NO_2 formation via ($NO + O_2$) reaction during lean-NO_x catalysis is not the rate-determining step. It further suggests that the critical role of O_2 in lean-NO_x catalysis is not NO_2 formation from NO but must be the oxidation (or partial oxidation) of hydrocarbons. Then, the next question is whether the C_2H_4 oxidation by O_2 can be the rate-determining step. In view of the kinetic isotope effect of NO demonstrated in this work, the C_2H_4 oxidation cannot be the rate-determining step. (If the C_2H_4 oxidation is the rate-determining step, the substitution of $^*NO$ for NO should not make any difference in the observed kinetics.) Thus, we conclude that the rate determining step of the lean-NO_x catalysis is the NO decomposition under the conditions of our experiments.

Model Predictions vs Experimental Data

Some discrepancy between model predictions and experimental data shown in Fig. 3 can be attributed in part to the nonuniformity of Pt surface phases along the axial distance of the reactor bed. It is most likely that the Pt surface phase in the reactor bed is not uniformly the (1×1)

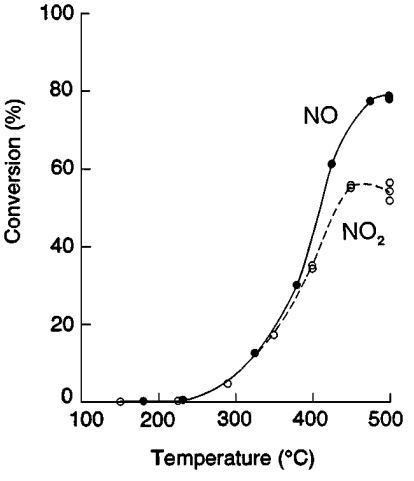

FIG. 10. Comparison of NO_x conversion efficiency in ($NO + C_2H_4$) and ($NO_2 + C_2H_4$) reactions (catalyst = 0.9 wt% Pt-ZSM-5, sample amount = 10.5 mg, total gas flow rate = 50 cc/m, feed concentrations = 230 ppm NO or NO_2, 1200 ppm C_2H_4).

or (hex) phases, even though the model implicitly assumed either a uniform (1×1) or (hex) phase for the entire reactor. In reality, the upstream section of the reactor may have the (1×1) phase while the downstream section may have the (hex) phase, due to the nonuniform distribution of the surface coverage of NO. This may partially explain why the upper limit of the NO conversion predicted by the model is higher (and its lower limit is lower) than the experimental data in Fig. 3.

Another source of the discrepancy may be the adsorptive isotope effect which was assumed negligible in the kinetic analysis. To the best of our knowledge, a quantitative description of adsorptive isotope effect applicable to our reaction system is not available in the literature. However, it is qualitatively established in general that the heavier an isotope molecule, the greater its adsorption equilibrium constant under the otherwise identical conditions (45). For the SV model which is applicable to the (1×1) phase, this means the adsorptive isotope effect enhances the kinetic isotope effect due to the greater value of $^*K$ (for *NO) compared with that of K (See Eq. [21]). This may also be part of the reason behind the discrepancy between the model predictions and the experimental data of the upper bound of the oscillation shown in Fig. 3. For the LH model which is applicable to the (hex) phase, the increase in the K value (due to *NO) can enhance or diminish the kinetic isotope effect depending on the value of KC (See Eq. [13]). Thus, it is not simple to predict the adsorptive isotope effect on the (hex) phase, because the KC value varies along the length of the reactor.

Obviously, the model predictions of the upper and lower bounds of the oscillations shown in Fig. 3 are based on complete microscopic synchronization of all parts of surfaces, including temperature and surface coverages. In reality, however, it is reasonable to expect only partial synchronization, somewhere between complete synchronization and and complete asynchronization. This may help explain why the observed oscillations are more complex than a single wave pattern, exhibiting some peaks with varying amplitudes smaller than the possible maximum (1).

Why Can *NO Initiate the Kinetic Oscillation While NO Cannot?

Figure 9a is a schematic diagram of Fig. 3, which illustrates a hysteresis loop involving the (1×1) and (hex) phases of Pt surfaces in the plane of NO conversion versus temperature. Noteworthy is that the (hex) phase is favored in the low temperature regime below the lower bifurcation temperature, while the (1×1) phase is favored in the high temperature regime above the upper bifurcation temperature. This is in sharp contrast to the bifurcation phenomenon reported for the $(NO + CO)$ reaction system on Pt (100) surfaces (32). As illustrated in Fig. 9b which is a schematic diagram of the experimental data reported in Ref. (32), for the $(NO + CO)$ reaction the (1×1) phase is favored in the low temperature regime while the (hex) phase is favored in the high temperature regime. This interesting difference in NO reduction kinetics between the $(NO + CO)$ reaction over Pt (100) and the $(^*NO + C_2H_4 + O_2)$ reaction over Pt-ZSM-5 may provide a clue to our question why *NO can initiate the kinetic oscillation while NO cannot under the otherwise identical conditions, as will be discussed in the following.

For the high temperature regime above the upper bifurcation temperature, the Pt surface has low adsorbate coverage for the $(NO + CO)$ system due to the fast surface reaction and desorption of NO and CO. This low surface coverage of NO and CO leads to the phase transition from (1×1) to (hex). On the other hand, for the $(^*NO + C_2H_4 + O_2)$ system, the reaction is not as fast as the $(NO + CO)$ reaction, resulting in a fairly high surface coverage of reactants, especially oxygen which is in large excess and known as a promoter for the phase transition like NO and CO (32). This sustained surface coverage of reactants stabilizes the (1×1) phase, and the transition from the (1×1) to the (hex) phase cannot initiate even at this high temperature.

For the low temperature regime below the lower bifurcation temperature, adsorption of NO and CO in the $(NO + CO)$ system immediately induces phase transition from the clean (hex) phase to the (1×1) phase. On the other hand, for the $(^*NO + C_2H_4 + O_2)$ system, the strong inhibition effect of *NO on the rate of the $(^*NO + C_2H_4 + O_2)$ reaction results in the high surface coverage of reactants, especially C_2H_4, due to a high concentration of C_2H_4 in the zeolite micropores. (Note that ZSM-5 has a large storage capacity for C_2H_4 in its micropore space (23).) Since hydrocarbons are known to retard the phase transition from the (hex) to (1×1) phase, the Pt surfaces remain (hex) until the surfaces are cleared of HC at around the lower bifurcation temperature which is close to the reaction lightoff temperature. In fact, the competition between the promoting effect of NO adsorption on the phase transition and the retarding effect of C_2H_4 adsorption may be the main cause of the observed kinetic oscillation. This is consistent with the observation that the kinetic oscillation stops when complete oxidation of C_2H_4 is achieved. (It may be worth noting that only steady-state multiplicities (without kinetic oscillation) could be observed for the $(NO + CO)$ reaction under the conditions where the bifurcation phenomenon occurred as shown in Fig. 9b (32).) This explanation is also consistent with our earlier observations which revealed a strong correlation between the kinetic isotope effect and the NO/C_2H_4 ratio in the feed (26).

In the case of the $(NO + C_2H_4 + O_2)$ system, the inhibition effect of NO is rather weak, compared with that of *NO. This leads to a faster reaction rate and thus a lower surface coverage of C_2H_4, compared with the $(^*NO_2 + C_2H_4 + O_2)$ system. The lower surface coverage of C_2H_4 may, in turn, eliminate the retardation effect of C_2H_4 on the phase

transition process from the (hex) to the (1×1), immediately inducing the phase transition from the (hex) to (1×1) due to adsorbed NO. This may explain why *NO can yield the kinetic oscillations while NO cannot under the same experimental conditions, as we have shown previously (1).

SUMMARY AND CONCLUSIONS

The effects of an NO isotope on the kinetics of lean-NO_x reduction over Pt-ZSM-5 were theoretically analyzed using a mechanistic model in which NO decomposition is assumed to be the rate-limiting step. Use of either NO or *NO in this comparative kinetic study enabled us to semi-isolate the NO decomposition process from the rest (such as C_2H_4 oxidation) during lean-NO_x catalysis. It has been demonstrated that the kinetic model, assuming the NO decomposition as the rate-determining step can adequately describe the experimental observations in terms of kinetic isotope effect, is indicative of the importance of the NO decomposition kinetics in the overall lean-NO_x catalysis. This finding is in support of the lean-NO_x reduction mechanism we recently proposed, which involves a combination of HC oxidation and NO decomposition (26). Results have also shown that the strong ^{15}NO isotope effects on lean-NO_x reduction kinetics can be explained by a combination of the primary and secondary isotope effects on NO decomposition kinetics over Pt surfaces which undergo adsorbate-induced phase transition between (1×1) and (hex) phases. The large kinetic isotope effect combined with kinetic oscillation appears to be the unique kinetic characteristic of lean-NO_x catalysis over Pt-ZSM-5, which exhibits a strong inhibition effect of NO. This finding bears an important implication in the reaction mechanism of the lean-NO_x catalysis over noble metal catalysts. More specific findings are

1. There are two sources of the kinetic isotope effects on lean-NO_x catalysis in a packed-bed reactor: primary and secondary effects. The primary effect is the quantum mechanical effect of the isotope on the zero-point vibrational energy level of NO molecules. The secondary effect is due to the change of surface coverages resulting from the primary effect along the reactor length. Due to this secondary effect, the overall kinetic isotope effect is much more complex and pronounced than the primary effect alone.
2. Results of the model predictions are in good quantitative agreement with the experimental data; the upper limit of the kinetic oscillation can be described by the rate of NO decomposition on the (1×1) phase, while the lower limit by that on the (hex) phase of the Pt surface.
3. The ability of the model to explain the isotope-induced kinetic oscillations suggests that NO decomposition may indeed be the rate-determining step in lean-NO_x catalysis over Pt-ZSM-5, in support of our previously proposed reaction mechanism that involves NO decomposition and HC oxidation.

This study provides an explanation for the large effect of an NO isotope on the kinetic behavior of Pt-ZSM-5 observed previously during lean-NO_x catalysis. It is hoped that results of this study will establish a sound basis on which to develop a complete kinetic model for lean-NO_x reduction over noble metal surfaces.

APPENDIX A: NOMENCLATURE

c = speed of light, 2.9979×10^{10} cm/s
C = gas-phase concentration of NO in the reactor, mol/cm^3
E = activation energy of the overall rate constant for NO decomposition ($\sigma_A k$), cal/mol
h = Planck constant, 6.6256×10^{-27} erg · s
k = decomposition rate constant of NO based on normalized surface coverages, mol/(cm^2 · s)
k' = decomposition rate constant of NO based on regular surface coverages, mol/(cm^2 · s)
k_a = adsorption rate constant of NO, cm^3/(mol · s)
k_d = desorption rate constant of NO, s^{-1}
K = adsorption equilibrium constant of NO, cm^3/mol
L = total reactor length, cm
Q = volumetric gas flow rate, cm^3/s
R = rate of NO decomposition, mol/(cm^2 · s)
R_g = ideal gas constant
T = absolute temperature, K
x = fractional conversion of NO
z = axial distance along the reactor, cm

Greek letters

α = dimensionless rate constant for NO decomposition defined by Eq. [15]
ε = activation energy of α, cal/mol
θ = surface coverage based on the total surface area
κ = Boltzmann constant, 1.3805×10^{-16} erg/K
μ = reduced mass of NO defined by $m_N m_O/(m_N + m_O)$, where m_N and m_O are the mass of nitrogen and oxygen atoms, respectively, g
ν = vibrational wave number of NO, cm^{-1}
ξ = dimensionless axial distance along the reactor, z/L
σ = total catalytic surface area, cm^2
σ_A = catalytic surface area of the A-sites, cm^2
$\langle \sigma_A \rangle$ = reactor-average value of σ_A, cm^2
σ_B = catalytic surface area of the B-sites, cm^2
ϕ = normalized surface coverage based on the surface area of type A

Subscripts

H = (hex) phase of Pt surface
HC = ethylene
e = exit condition
i = inlet condition

N = nitrogen atom on the surface
NO = nitric oxide
O = oxygen
V = vacancy
11 = (1×1) phase of Pt surface

Superscript

$*$ = associated with the ^{15}NO isotope

APPENDIX B: DERIVATION OF EXPRESSION FOR NORMALIZED SURFACE COVERAGE

Equilibrium of adsorption/desorption process for NO on type A-sites can be described by

$$k_a C\theta_V - k_d\theta_{NO} = 0, \qquad [B.1]$$

which, with the help of Eq. [2], can be written as

$$KC(1-\theta_O-\theta_{HC}-\theta_N) = \theta_{NO}(1+KC). \qquad [B.2]$$

Rearrangement of Eq. [B.2] yields

$$\frac{KC}{1+KC} = \frac{\theta_{NO}}{1-\theta_O-\theta_{HC}-\theta_N} \equiv \phi_{NO}. \qquad [B.3]$$

Noting that

$$1-\theta_O-\theta_{HC}-\theta_N = \theta_{NO}+\theta_V, \qquad [B.4]$$

we obtain from Eq. [B.3]

$$1-\phi_{NO} = 1-\frac{\theta_{NO}}{\theta_{NO}+\theta_V} = \frac{\theta_V}{\theta_{NO}+\theta_V} = \frac{1}{1+KC}. \qquad [B.5]$$

Then, by the definition of the normalized surface coverage,

$$\phi_V \equiv \frac{\theta_V}{\theta_{NO}+\theta_V} = \frac{1}{1+KC}. \qquad [B.6]$$

APPENDIX C: DERIVATION OF EQ. [19] BY FIRST ORDER PERTURBATION

For simplicity and generalization, Eq. [16] can be rewritten as

$$\frac{1}{2}[(2+KC_i)^2-(2+KC_e)^2]+\ln\left(\frac{C_i}{C_e}\right) = \alpha, \qquad [C.1]$$

where C_e is the gas-phase concentration of NO at the reactor exit. Perturbation of α and C_e by a small amount of $\delta\alpha$ and δC_e, respectively, yields

$$\frac{1}{2}[(2+KC_i)^2-\{2+K(C_e+\delta C_e)\}^2] + \ln\left(\frac{C_i}{C_e+\delta C_e}\right) = \alpha+\delta\alpha. \qquad [C.2]$$

Using Eq. [C.1] while neglecting the second order terms in δC_e, we can reduce Eq. [C.2] to

$$K(2+KC_e)\delta C_e + \ln\left(1+\frac{\delta C_e}{C_e}\right) = -\delta\alpha, \qquad [C.3]$$

which can be further reduced to

$$\frac{\delta C_e}{C_e}(1+KC_e)^2 = -\delta\alpha, \qquad [C.4]$$

since $\ln(1+\delta C_e/C_e)$ can be approximated by $\delta C_e/C_e$ for a small perturbation. Noting that

$$\frac{\delta C_e}{C_e} = \frac{C_e^*}{C_e}-1, \qquad [C.5]$$

$$\frac{\delta\alpha}{\alpha} = \frac{\alpha^*}{\alpha}-1, \qquad [C.6]$$

we can rearrange Eq. [C.4] to yield

$$\frac{C_e^*}{C_e}-1 = \frac{\alpha}{(1+KC_e)^2}\left(1-\frac{\alpha^*}{\alpha}\right). \qquad [C.7]$$

Furthermore, since $C_e = C_i(1-x)$ and $\alpha^*/\alpha = k^*/k$, Eq. [C.7] can be written as

$$\frac{C_i^*(1-x^*)}{C_i(1-x)} = 1+\frac{\alpha}{[1+KC_i(1-x)]^2}\left(1-\frac{k^*}{k}\right). \qquad [C.8]$$

REFERENCES

1. Cho, B. K., *J. Catal.* **157**, 14 (1995).
2. Held, W., Konig, A., Richter, T., and Puppe, L., SAE Paper 900496 (1990).
3. Iwamoto, M., and Hamada, H., *Catal. Today* **10**, 57 (1991).
4. Montreuil, C. N., and Shelef, M., *Appl. Catal. B* **1**, L1 (1992).
5. Li, Y., and Armor, J. N., *Appl. Catal. B* **1**, L31 (1992).
6. Zhang, G., Yamaguchi, T., Kawakami, H., and Suzuki, T., *Appl. Catal. B* **1**, L15 (1992).
7. Hirabayashi, H., Yahiro, H., Mizuno, N., and Iwamoto, M., *Chem. Lett.*, 2235 (1992).
8. Truex, T. J., Searles, R. A., and Sun, D. C., *Platinum Met. Rev.* **36**, 2 (1992).
9. Bennett, C. J., Bennett, P. S., Golunski, S. E., Hayes, J. W., and Walker, A. P., *Appl. Catal. A* **86**, L1 (1992).
10. Cho, B. K., *J. Catal.* **142**, 418 (1993).
11. Monroe, D. R., DiMaggio, C. L., Beck, D. D., and Matekunas, A., SAE Paper 930737 (1993).
12. Kharas, K. C. C., Robota, H. J., and Liu, D. J., *Appl. Catal. B* **2**, 225 (1993).
13. Ansell, G. P., Diwell, A. F., Golunski, S. E., Hayes, J. W., Rajaram, R. R., Truex, T. J., and Walker, A. P., *Appl. Catal. B* **2**, 81 (1993).
14. d'Itri, J. L., and Sachtler, M. H., *Appl. Catal. B* **2**, L7 (1993).
15. Obuchi, A., Ohi, A., Nakamura, M., Ogata, A., Mizuno, K., and Obuchi, H., *Appl. Catal. B* **2**, 71 (1993).
16. Engler, B. H., Leyrer, J., Lox, E. S., and Ostgathe, K., SAE Paper 930735 (1993).
17. Heinrich, M. J., and Deviney, M. L., SAE Paper 930736 (1993).
18. Li, Y., and Armor, J. N., *Appl. Catal. B* **3**, 55 (1993).

19. Petunchi, J. O., Sill, G., and Hall, W. K., *Appl. Catal. B* **2**, 303 (1993).
20. Bethke, K. A., Alt, D., and Kung, M. C., *Catal. Lett.* **25**, 37 (1994).
21. Burch, R., and Scire, S., *Appl. Catal. B* **3**, 295 (1994).
22. Burch, R., Millington, P. J., and Walker, A. P., *Appl. Catal. B* **4**, 65 (1994).
23. Cho, B. K., *J. Catal.* **155**, 184 (1995).
24. Bethke, K. A., Li, C., Kung, M. C., Yang, B., and Kung, H. H., *Catal. Lett.* **31**, 287 (1995).
25. Takami, A., Takemoto, T., Iwakuni, H., Saito, F., and Komatsu, K., SAE Paper 950746 (1995).
26. Cho, B. K., and Yie, J. E., *Appl. Catal. B* **10**, 263 (1996).
27. Cho, B. K., *Appl. Catal. B* **12**, 147 (1997).
28. Obuchi, A., Nakamura, M., Ogata, A., Mizuno, K., Ohi, A., and Obuchi, H., *J. Chem. Soc., Chem. Commun.*, 1150 (1992).
29. Melander, L., "Isotope Effects on Reaction Rates," Ronald Press, New York, 1960.
30. Bonzel, H. P., Broden, G., and Pirug, G., *J. Catal.* **53**, 96 (1978).
31. Gorte, R. J., Schmidt, L. D., and Gland, J. L., *Surf. Sci.* **109**, 367 (1981).
32. Schwartz, S. B., and Schmidt, L. D., *Surf. Sci.* **206**, 169 (1988).
33. Morrow, B. A., Chevrier, J. P., and Moran, L. E., *J. Catal.* **91**, 208 (1985).
34. Wang, T., Lee, C., and Schmidt, L. D., *Surf. Sci.* **163**, 181 (1985).
35. Schwartz, S. B., and Schmidt, L. D., *Surf. Sci.* **183**, L269 (1987).
36. Gardner, P., Tushaus, M., Martin, R., and Bradshaw, A. M., *Surf. Sci.* **240**, 112 (1990).
37. Veser, G., Esch, F., and Imbihl, R., *Catal. Lett.* **13**, 371 (1992).
38. Lombardo, S. J., Fink, T., and Imbihl, R., *J. Chem. Phys.* **98**, 5526 (1993).
39. Fink, Th., Dath, J.-P., Bassett, M. R., Imbihl, R., and Ertl, G., *Surf. Sci.* **245**, 96 (1991).
40. Cho, B. K., unpublished results, 1997.
41. Ong, B. G., and Mason, D. M., *Ind. Eng. Chem. Fund.* **11**, 169 (1972).
42. Papapolymerou, G. A., and Schmidt, L. D., *Langmuir* **1**, 488 (1985).
43. Sasaki, M., Hamada, H., Kintaichi, Y., and Ito, T., *Catal. Lett.* **15**, 297 (1992).
44. Bethke, K. A., Li, C., Kung, M. C., Yang, B., and Kung, H. H., *Catal. Lett.* **31**, 287 (1995).
45. Haubach, W. J., Radhakrishna, P., Katorski, A., Wang, R., and White, D., *in* "Advances in Chemistry Series, Vol. 89: Isotope Effects in Chemical Processes" (R. F. Gould, Ed.), Am. Chem. Soc., Washington, DC, 1969.